Title

A missense mutation in ASRGL1 is involved in causing autosomal recessive retinal degeneration

Journal

Human Molecular Genetics, 25(12)

ISSN

0964-6906

Authors

Biswas, Pooja
Chavali, Venkata Ramana Murthy
Agnello, Giulia
et al.

Publication Date

2016-06-15

DOI

10.1093/hmg/ddw113

Peer reviewed

Human Molecular Genetics, 2016, Vol. 25, No. 12 2483–2497

doi: 10.1093/hmg/ddw113
Advance Access Publication Date: 22 April 2016
Original Article

ORIGINAL ARTICLE

A missense mutation in *ASRGL1* is involved in causing autosomal recessive retinal degeneration

Pooja Biswas[1], Venkata Ramana Murthy Chavali[1,2], Giulia Agnello[3], Everett Stone[3], Christina Chakarova[4], Jacque L. Duncan[5], Chitra Kannabiran[6], Melissa Homsher[2], Shomi S. Bhattacharya[4], Muhammad Asif Naeem[7], Adva Kimchi[8], Dror Sharon[8], Takeshi Iwata[9], Shaikh Riazuddin[10,11], G. Bhanuprakash Reddy[12], J. Fielding Hejtmancik[13], George Georgiou[3], S. Amer Riazuddin[14,*] and Radha Ayyagari[1,*]

[1]Shiley Eye Institute, University of California San Diego, La Jolla, CA, USA, [2]Ophthalmology, University of Pennsylvania, Philadelphia, PA, USA, [3]Departments of Biomedical and Chemical Engineering, Molecular Biosciences, Section of Molecular Genetics and Microbiology, and Institute for Cell and Molecular Biology, The University of Texas at Austin, Austin, TX, USA, [4]UCL Institute of Ophthalmology, 11-43 Bath Street, London, UK, [5]Ophthalmology, University of California San Francisco, San Francisco, CA, USA, [6]Kallam Anji Reddy Molecular Genetics Laboratory, L V Prasad Eye Institute (LVPEI), Kallam Anji Reddy Campus, L V Prasad Marg, Hyderabad 500 034, India, [7]National Centre of Excellence in Molecular Biology, University of the Punjab, Lahore, Pakistan, [8]Department of Ophthalmology, Hadassah-Hebrew University Medical Center, Jerusalem, Israel, [9]Division of Molecular and Cellular Biology, National Institute of Sensory Organs, National Hospital Organization Tokyo Medical Center, Tokyo, Japan, [10]Allama Iqbal Medical College, University of Health Sciences Lahore, Pakistan, [11]National Centre for Genetic Diseases, Shaheed Zulfiqar Ali Bhutto Medical University, Islamabad, Pakistan, [12]National Institute of Nutrition, Hyderabad 500 007, India, [13]OMGS/OGVFB branch, National Eye Institute, NIH, Bethesda, MD, USA and [14]The Wilmer Eye Institute, Johns Hopkins University School of Medicine, Baltimore, MD, USA

*To whom the correspondence should be addressed at: Shiley Eye Institute, University of California San Diego, 9415 Campus Point Drive, JRC 206, La Jolla, California, USA. Tel: (858) 534-9029; Fax: (858) 246-0568; E-mail: rayyagari@ucsd.edu (R.A.); The Wilmer Eye Institute, John Hopkins University School of Medicine, Baltimore, MD, USA, Tel: 410-955-3656; E-mail: riazuddin@jhmi.edu (S.A.R.)

Abstract

Inherited retinal dystrophies are a group of genetically heterogeneous conditions with broad phenotypic heterogeneity. We analyzed a large five-generation pedigree with early-onset recessive retinal degeneration to identify the causative mutation. Linkage analysis and homozygosity mapping combined with exome sequencing were carried out to map the disease locus and identify the p.G178R mutation in the asparaginase like-1 gene (*ASRGL1*), segregating with the retinal dystrophy phenotype in the study pedigree. *ASRGL1* encodes an enzyme that catalyzes the hydrolysis of L-asparagine and isoaspartyl-peptides. Studies on the *ASRGL1* expressed in *Escherichia coli* and transiently transfected mammalian cells indicated that the

Received: January 28, 2016. **Revised:** March 22, 2016. **Accepted:** April 11, 2016

p.G178R mutation impairs the autocatalytic processing of this enzyme resulting in the loss of functional ASRGL1 and leaving the inactive precursor protein as a destabilized and aggregation-prone protein. A zebrafish model overexpressing the mutant h*ASRGL1* developed retinal abnormalities and loss of cone photoreceptors. Our studies suggest that the p.G178R mutation in *ASRGL1* leads to photoreceptor degeneration resulting in progressive vision loss.

Introduction

Inherited retinal degenerations (IRDs) are a group of conditions that result in irreversible loss of vision. Clinical symptoms of retinal degenerations commonly include night blindness and loss of central or peripheral vision at initial stages, which may progress to complete blindness at later stages (1). Primary pathology often involves degeneration of photoreceptors or retinal pigment epithelium (RPE) cells (2). Retinal degenerations are inherited in autosomal dominant, autosomal recessive, X-linked, mitochondrial and complex modes. Broad phenotypic and genetic heterogeneity has been reported in patients/families with hereditary retinal conditions (3–6). More than 80 genes have been established to be involved in causing retinitis pigmentosa, a common form of IRD (RetNet. In http://www.sph.uth.tmc.edu/Retnet).

Autosomal recessive retinal degenerations are more common in populations with high rates of consanguinity. Mutations in several genes implicated in causing IRD have been identified in patients from Pakistan with high consanguinity (7–15). However, no single mutation or single gene contributing to a significant proportion of IRD cases in this population has been observed, indicating that the underlying cause of these degenerations in this population is genetically heterogeneous.

In this study, we describe the identification of a mutation in the novel gene asparaginase like-1 (*ASRGL1*) as the underlying cause of IRD in a five-generation consanguineous pedigree from Pakistan.

Results

Clinical analysis

Individuals IV:1, IV:3, IV:7, and IV:8 underwent ophthalmic evaluation (Fig. 1). Fundus examination revealed retinal vessel attenuation and pigmentation in affected members IV:1 and IV:8, with macular RPE atrophy in IV:1 (Fig. 2). Night blindness was reported to be the first symptom of disease in all affected members. Scotopic responses at 0 db and photopic 30 Hz flicker responses were undetectable in affected individuals, demonstrating compromised rod and cone photoreceptor function, while unaffected individuals exhibited rod and cone responses within normal ranges (Fig. 3). Onset of vision abnormalities in affected members was reported to be between 5 and 8 years of age (Table 1).

Genome-wide linkage analysis

The large numbers of enrollment (six-affected individuals in two consanguineous matings) augmented the power of the family to generate statistically significant two-point LOD scores during genome-wide linkage. Our theoretical estimates confirmed that PKRD104 could attain a maximum two-point LOD score of 5.25 (at $\theta = 0$). Subsequently, we completed a genome-wide scan and calculated two-point LOD scores that localized the disease phenotype to chromosome 11q with a two-point LOD score of 3.23 with marker D11S4191 (at $\theta = 0$). Analysis of additional Short Tandem Repeat (STR) markers in that region yielded two-point LOD scores of 5.06, 1.99, and 5.22 with D11S4459, D11S2006, and D11S1765 (Table 2). The haplotype constructed from alleles of STRs further supported localization of the IRD locus in PKRD104 to chromosome 11q. As shown in Figure 1, there is a proximal recombination at D11S905 in individual IV:8, and distal recombination in individual IV:7 at D11S1883, and individual IV:6 at marker D11S987. In addition, affected individuals IV:1, IV:5, IV:6, IV:7 and V:1 are heterozygous for alleles of D11S905. Taken together, this localizes the disease gene to a 13.1 cM (22.65 Mb) interval on chromosome 11q flanked by markers D11S905, proximally, and D11S1883, distally (Fig. 1).

Candidate gene analysis

Screening the disease gene interval on chromosome 11 revealed the presence of a previously reported retinal disease gene, Bestrophin-1 (BEST1/VMD2), associated with Best macular degeneration and recessive bestrophinopathy (16–19). Although the clinical signs or symptoms of our patients were different from classical Best macular degeneration, affected members IV-8 and IV-9 were screened for the presence of *BEST1* gene mutations and none were observed, suggesting the possible involvement of a novel gene in causing retinal degeneration. Examination of the exome sequence did not reveal large deletions in the *BEST1* gene.

Exome sequencing and analysis of variants

Exomes of two affected (IV:7 and IV:8) and one unaffected member (IV:2) of the PKRD104 pedigree were captured (Fig. 1) and variants were identified. A total of 4641 homozygous variants including Single Nucleotide Polymorphism and Insertion Deletion were present in both affected members in the homozygous state and absent or heterozygous in the unaffected member (IV:2). Among these, 503 were rare (<0.003) or novel variants. Forty-nine of these variants were found to be in the coding region and only 13 of them were predicted to be pathogenic (Supplementary Material, Table S1). No intronic canonical splice variants were observed to be segregating with the phenotype in our study family. Segregation analysis of these variants identified a single missense change, c.532G > A in the *ASRGL1* gene segregating with retinal degeneration in PKRD104 (Fig. 1). This c.532G > A variant observed in the *ASRGL1* gene is predicted to be damaging by SIFT (0.00), probably damaging by PolyPhen2 (0.998) and also disease causing by Mutation Taster (0.999). The glycine residue is highly conserved in different species (Supplementary Material, Figure S1). This gene is located in the critical interval identified by linkage and haplotype analyses. This variant is not listed in both the 1000 genomes and ExAC database. This variant was absent in 1790 unaffected individuals (150 ethnicity-matched controls, 300 Caucasian controls and 1340 unaffected individuals of Arab ancestry). Examination of the exome sequence data of individuals affected with IRD and from Pakistani (117 individuals), Indian (80 individuals), Middle Eastern (48 individuals), Arabic (208 individuals), Caucasian (350 individuals) and Japanese (618 individuals) populations did not detect c.532G > A or additional causative mutations in the *ASRGL1* gene. This suggests that, c.532G > A variant in *ASRGL1* is rare and this mutation in this

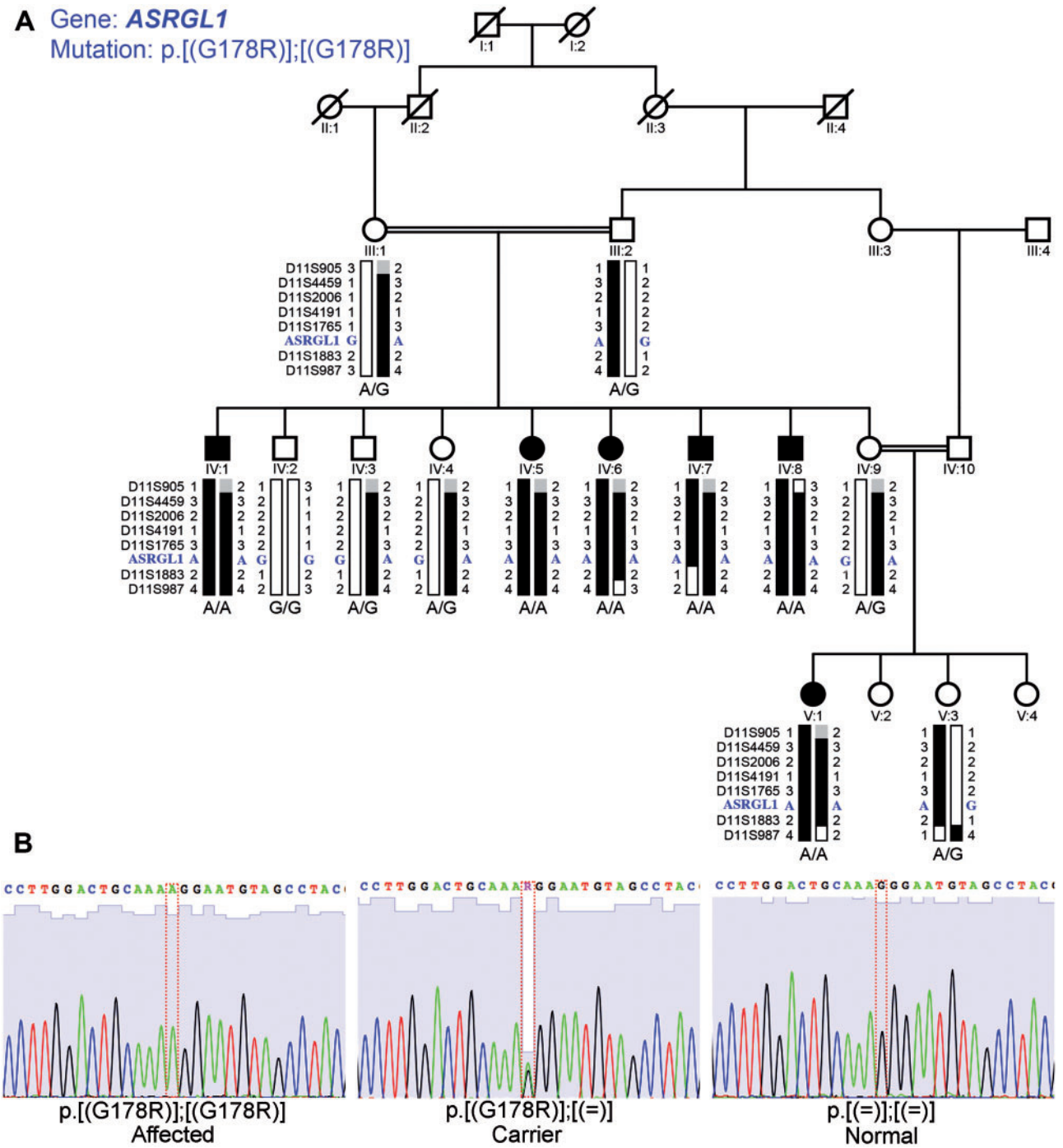

Figure 1. (**A**) Haplotype analysis and segregation of the *ASRGL1* p.G178R mutation in a five-generation pedigree with recessive IRD: haplotype was constructed with the genotypes of 7 microsatellite markers and identified D11S4459 and D11S1883 markers as the boundaries of the disease interval on chromosome 11 (q12.1–q13.1). The p.G178R *ASRGL1* mutation segregated with IRD in this pedigree. **(B)** Sequence of the region encompassing the *ASRGL1* p.G178R mutation in an affected, carrier and unaffected individual from the pedigree with IRD.

gene may not contribute to a significant proportion of cases with IRD in these populations.

Expression profile of *ASRGL1*

Among the ocular tissues tested, high levels of *ASRGL1* transcript was observed in the optic nerve and retina while relatively low levels of expression were noted in the iris-ciliary body, lens or RPE of 2-months-old wild type (wt) C57BL/6 mice (Fig. 4A). The *ASRGL1* transcript expression levels increased steadily in the retina from P14 to P60 and sustained high levels of this transcript were noted in the adult retina at the age of six months (Fig. 4B). High levels of expression of *ASRGL1* transcript was observed in the heart and brain tissue of 2-months-old mouse while low to minimal expression was noted in the remaining tissue tested (Fig. 4C).

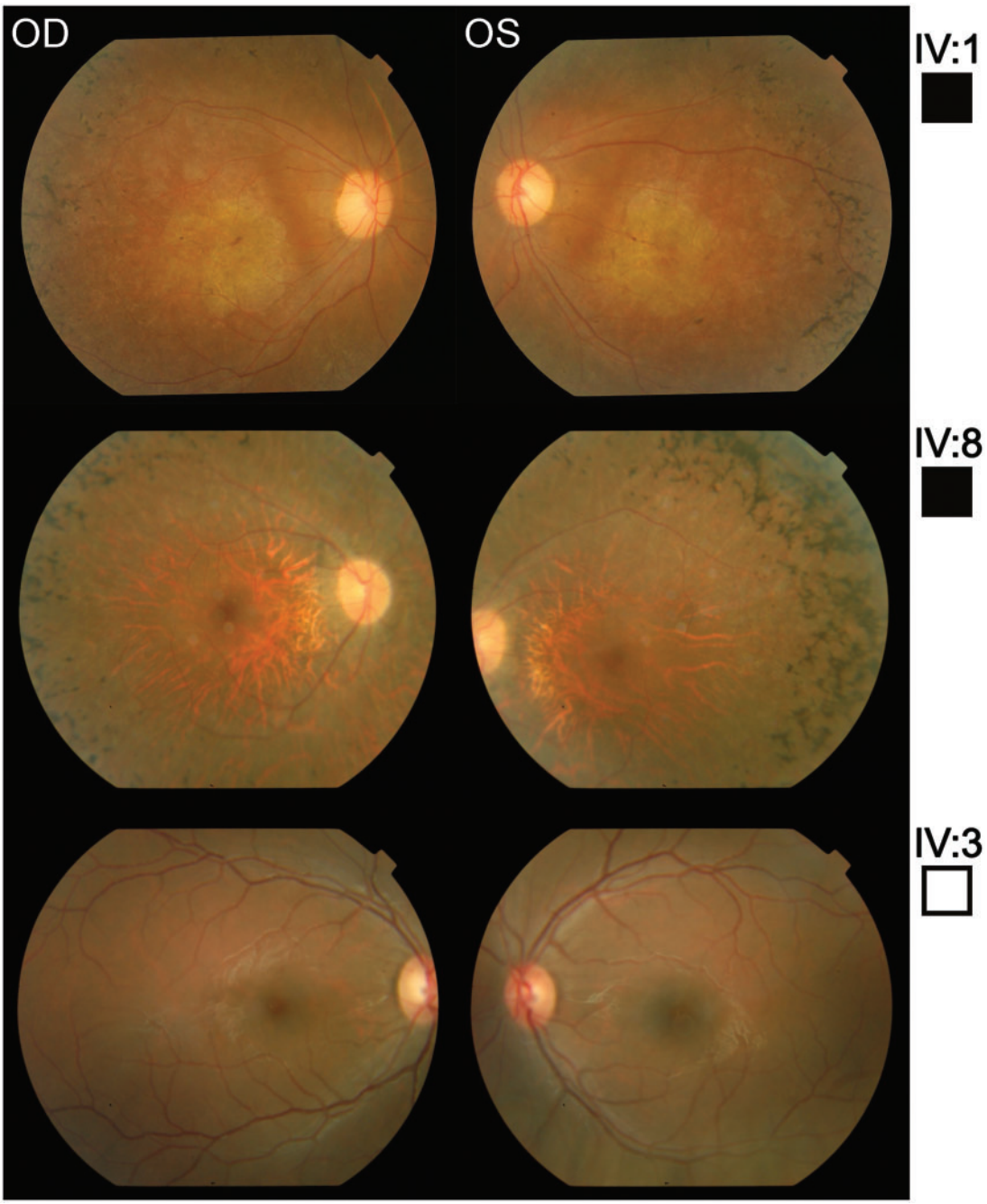

Figure 2. Fundus images of two affected and one unaffected member: Fundus images of affected members show retinal vessel attenuation, pigmentation (IV:1 30 years old and IV:8 50 years old) and a bull's eye pattern of RPE atrophy in IV:1. Whereas, the fundus images of the unaffected member IV:3 showed no abnormality.

Localization of ASRGL1 in the retina

Immunostaining of 2-months-old C57BL/6 mouse retinal sections with anti-ASRGL1 antibodies localized this protein to the photoreceptor inner segment region (Fig. 4D). The expression of ASRGL1 is found to be minimal to absent in other layers of the retina (Fig. 4D).

In vitro biochemical analysis of ASRGL1

The active form of ASRGL1 is generated by autocatalytic processing (20). To evaluate whether the p.G178R mutation alters either the autoprocessing or the asparaginase and/or isoaspartyl peptidase activity of this enzyme, the cDNA encoding wt-ASRGL1 and G178R-ASRGL1 sequences were tagged with nucleotides encoding an N-terminal His6 affinity tag and expressed from a T7 promoter in *Escherichia coli* (DE3) BL21 cells (20). Wt-ASRGL1 and G178R-ASRGL1 proteins were isolated by immobilized metal ion affinity chromatography and analyzed by sodium dodecyl sulfate-polyacrylamide gel electrophoresis (SDS-PAGE). Incubation of wt-ASRGL1 at 37 °C resulted in a reduction in the intensity of the full-length protein band (~38 kDa) over time, concomitant with an increase in two lower molecular weight bands (~23 and

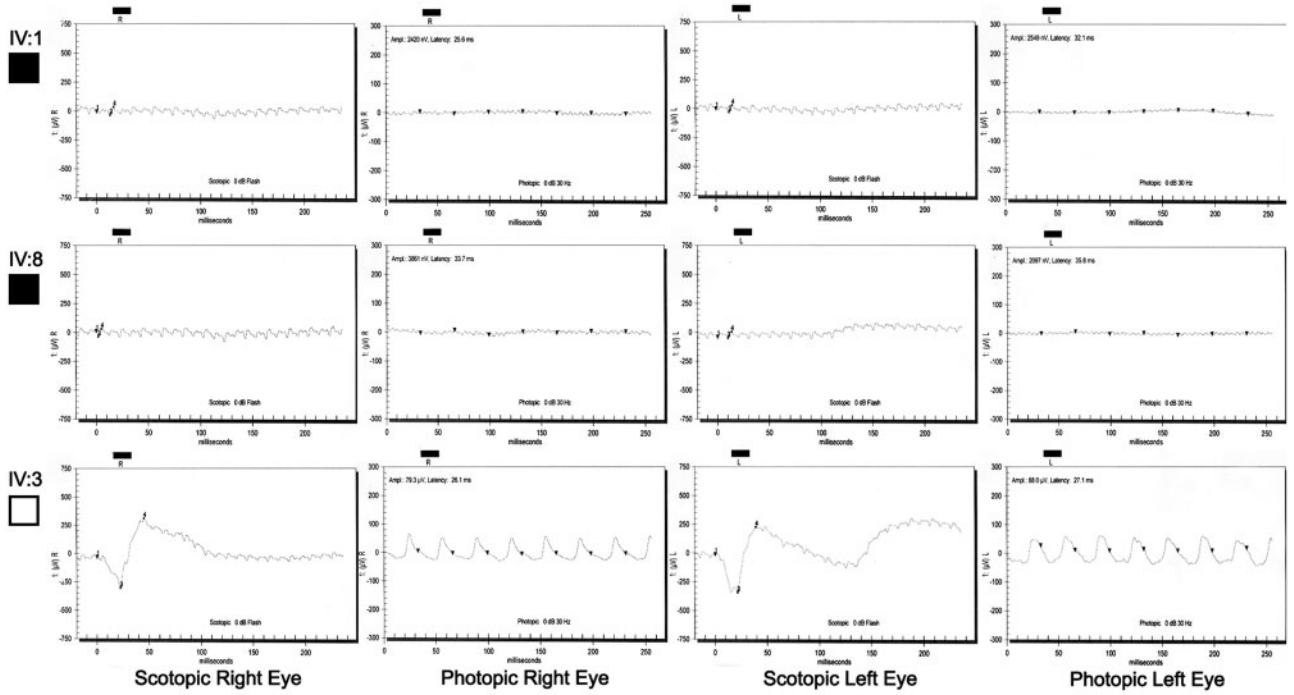

Figure 3. Full field ERG response in two affected and one unaffected member of the family with IRD. Scotopic responses at 0 db and 30 Hz flicker responses of affected members IV:1 (30 years old) and IV:8 (50 years old) were undetectable suggestive of compromised rod and cone photoreceptor response while the unaffected individual (IV:3) exhibited rod and cone responses within normal ranges.

Table 1. The clinical phenotype of affected members

ID	Sex	Age	Symptom	Age of onset	Fundus appearance	Lens abnormalities
IV: 1	M	30 years	Night blindness	8 years	Pigmentation, Retinal attenuation and Bull's eye pattern of RPE atrophy in the macula	NO
IV: 5	F	34 years	Night blindness	N/A	Pigmentation and Retinal attenuation	NO
IV: 6	F	32 years	Night blindness	N/A	Pigmentation and Retinal attenuation	NO
IV: 7	M	45 years	Night blindness	8 years	Pigmentation and Retinal attenuation	NO
IV: 8	M	50 years	Night blindness	7 years	Pigmentation and Retinal attenuation	NO

Note: N/A indicates 'Not Available'.

Table 2. Two-point LOD scores of chromosome 11q markers for family PKRD104

Markers	cM	Mb	0	0.01	0.05	0.07	0.1	0.2	0.3	Z_{max}	θ_{max}
D11S905*	51.95	40.95	$-\infty$	−0.438	−0.088	0.111	0.28	0.4	0.269	0.4	0.2
D11S4459	58.4	56.74	5.06	4.742	4.526	4.307	3.973	2.818	1.612	5.06	0
D11S2006	59.24	59.95	1.990	1.953	1.802	1.724	1.605	1.191	0.765	1.990	0
D11S4191*	60.09	60.23	3.239	3.02	2.871	2.721	2.494	1.718	0.939	3.239	0
D11S1765	61.78	61.01	5.228	4.909	4.693	4.474	4.14	2.983	1.776	5.228	0
D11S1883	65.05	63.6	$-\infty$	2.131	2.377	2.468	2.473	2.022	1.285	2.473	0.1
D11S987*	67.48	68.12	$-\infty$	1.73	1.813	1.818	1.759	1.336	0.791	1.818	0.07

Note: Asterisks (*) denote markers used in the genome-wide scan.

15 kDa), corresponding to the processed α and β subunits (Fig. 5A). In contrast, no evidence of processing over the same period of time was observed for G178R-ASRGL1 suggesting that the p.G178R mutation may impair the autocatalytic activity of ASRGL1. Additionally, incubation of G178R-ASRGL1 at 37 °C over time resulted in accumulation of high molecular weight (HMW) species indicating protein aggregation (Fig. 5A).

Data from SDS-PAGE gel densitometry (Fig. 5B and C) and size exclusion chromatography (data not shown) revealed that the unprocessed wt-ASRGL1 fraction partitions to HMW species, given the high instability of the unprocessed protein (21). Both unprocessed and processed fractions of G178R-ASRGL1 partition to HMW species. Further analysis revealed that the p.G178R substitution affects only autocatalytic processing and solubility

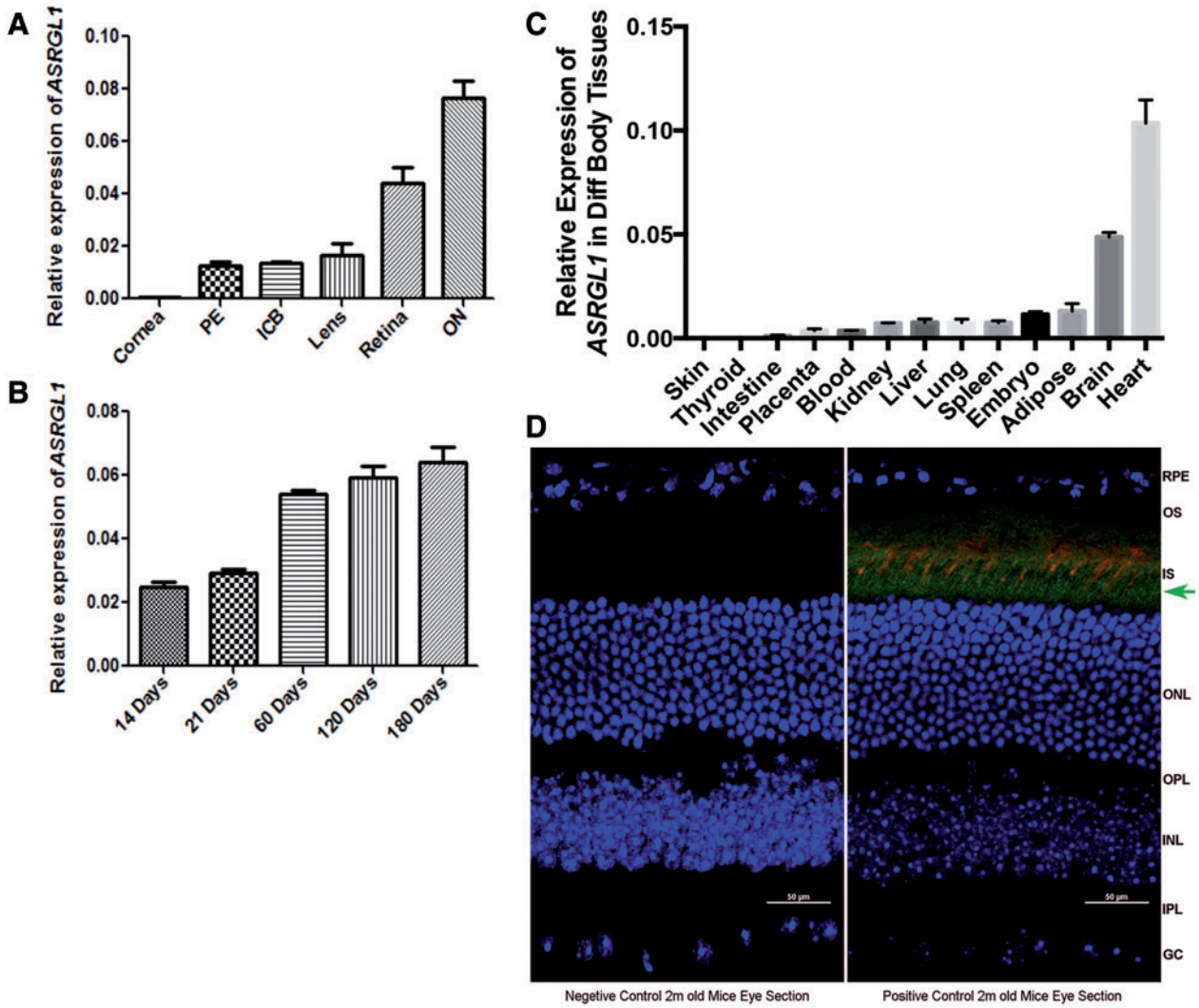

Figure 4. Expression profile of *ASRGL1* in ocular and body tissue. **(A)** Levels of expression of *ASRGL1* transcript in 2-months-old old mouse ocular tissue as measured by quantitative real-time PCR. PE: Posterior eye cup (RPE + Choroid); ICB: Iris-Ciliary body; ON: Optic nerve. **(B)** Expression of *ASRGL1* transcript in the retinal tissue of mice during development and aging as measured by quantitative real-time PCR. **(C)** Levels of expression of *ASRGL1* transcript in 2-months-old mouse different body tissue as measured by quantitative real-time PCR. **(D)** Immunostaining of 2 months old mouse retinal sections with only secondary antibodies did not reveal positive staining in the left image. Right side image representing the localization of ASRGL1 protein to the photoreceptor inner segment region of a 2-months-old mouse retina: ASRGL1 signal was represented by green fluorescence and red fluorescence color represented S-cones. RPE: Retinal pigment epithelium; OS: outer segments; IS: inner segments; ONL: outer nuclear layer; OPL: outer plexiform layer; INL: inner nuclear layer; IPL: inner plexiform layer; GC: ganglion cell layer.

and not the L-asparaginase nor the isoaspartyl peptidase activity of the enzyme. Circularly permutation of ASRGL1 allows to decouple auto processing from substrate hydrolysis (21). When comparing the hydrolysis of the L-asparagine substrate analogue, L-aspartic acid-β-hydroxamate (AHA) to the wt and mutant enzymes, both in the circularly permuted format (wt-(cp)ASRGL1 and G178R-(cp)ASRGL1), the k_{cat}/K_M values were not significantly different from each other ($P < 0.38$) (Table 3). In addition, the mutant in the circularly permuted format (G178R-(cp)ASRGL1) displays a preserved activity towards the isoaspartyl dipeptide, β-Asp-Phe methyl esther (Table 3). All together these findings suggest that the p.G178R mutation results in highly impaired autocatalytic processing of ASRGL1 causing the protein to aggregate, leaving only a small fraction of functional enzyme. This in turn may result in accumulation of isoaspartyl peptides and L-asparagine and the formation of protein aggregates.

Expression and localization of ASRGL1 in heterologous cells

Cos-7 cells transfected with mammalian constructs containing wt-*ASRGL1* (wt/wt) tagged with cMyc showed the distribution of ASRGL1-cMyc fusion protein throughout the cytoplasm, whereas cells transfected with constructs containing the mutant *ASRGL1* (mut/mut) showed juxtanuclear localization of the G178R-ASRGL1-cMyc signal. Staining these transfected cells with vimentin antibodies indicated re-organization of the cytoskeleton in cells expressing the mutant ASRGL1 (Fig. 6A–F, Supplementary Material, Figure S2A and B). Similar results were obtained when 293-A cells were transfected with the wt and G178R-*ASRGL1* constructs (data not shown). Mock-transfected cells did not have immunostaining. These observations suggest that the mutant ASRGL1 may form aggresomes and not be available to exert its normal function.

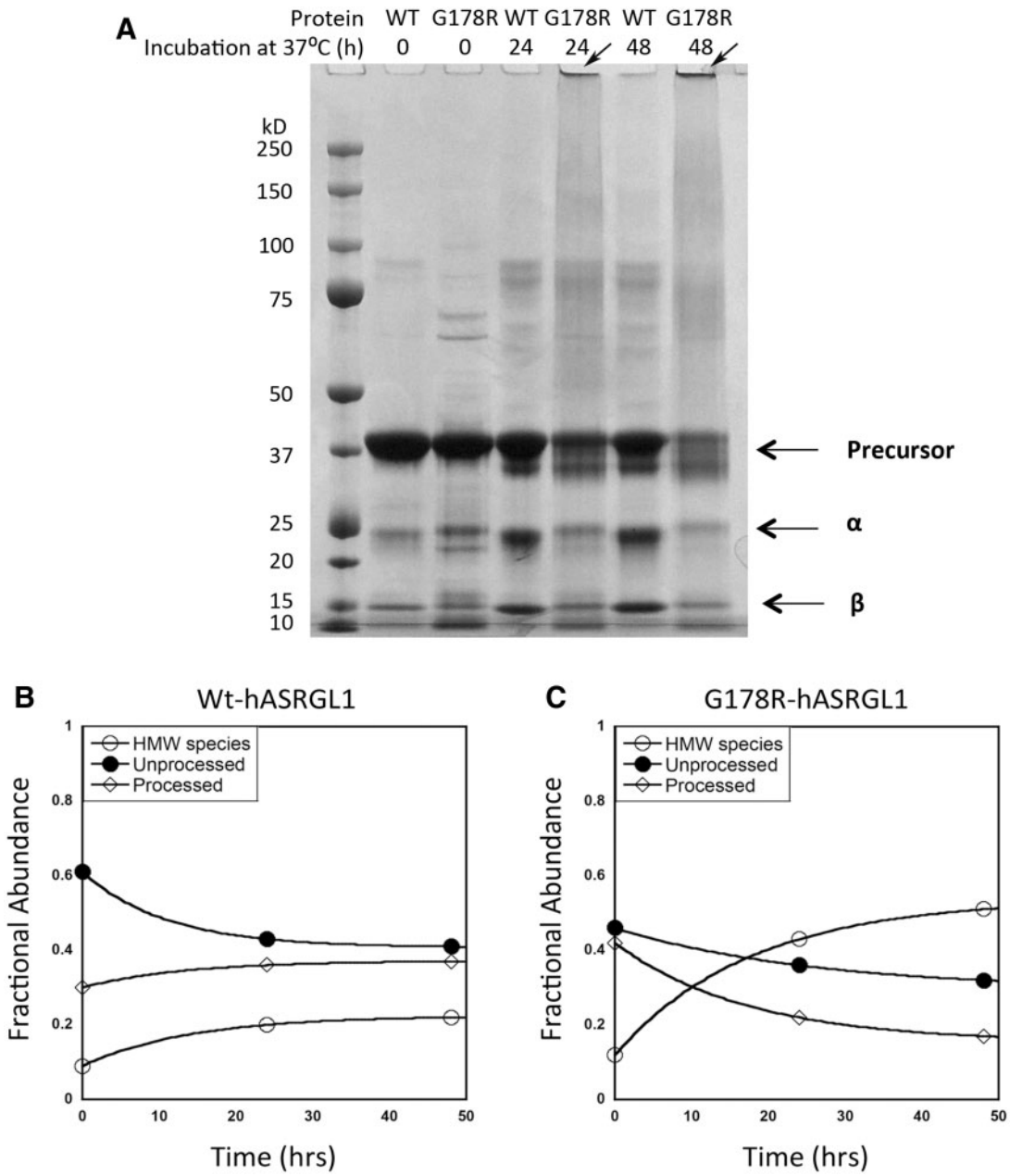

Figure 5. *In vitro processing of wt-ASRGL1and G178R-ASRGL1.* **(A)** SDS-PAGE of wt-ASRGL1 and G178R-ASRGL1 following *in vitro* incubation at 37 °C over time. HMW species in lanes (5 and 7) loaded with the G178R-ASRGL1 are indicated with arrows. **(B)** Densitometry analysis of intramolecular processing of wt-ASRGL1 and G178R-ASRGL1 following in vitro incubation at 37 °C over time.

Table 3. Summary of kinetic parameters of G178R-(cp)ASRGL1 hydrolysis of L-AHA

A. L-AHA hydrolysis			
Variant	k_{cat} (s^{-1})	K_M (mM)	k_{cat}/K_M ($mM^{-1}s^{-1}$)
wt-(cp)ASRGL1	1.8 ± 0.05	0.09 ± 0.01	20 ± 2.8
G178R-(cp)ASRGL1	1.8 ± 0.04	0.1 ± 0.01	18 ± 2.2
B. β-Asp-Phe methyl ester hydrolysis			
Variant	k_{cat} (s^{-1})	K_M (mM)	k_{cat}/K_M ($mM^{-1}s^{-1}$)
G178R-(cp)ASRGL1	7.5 ± 0.3	1.1 ± 0.1	6.8 ± 0.9

Asparaginase activity of ASRGL1

Asparaginase activity was measured in the whole cell lysates of 2×10^6 Cos-7 post-transfected cells with the wt-*ASRGL1* and G178R-*ASRGL1* plasmids to determine the effect of the p.G178R mutation on the enzymatic activity of ASRGL1. The asparaginase activity in the lysates of cells transfected with the G178R-*ASRGL1* or mock-transfected cells (Fig. 6G) was found to be minimal. Whereas the lysate of cells transfected with the wt-*ASRGL1* showed significantly higher asparaginase activity ($P < 0.0001$) compared with the lysates of cells expressing G178R-*ASRGL1* or mock-transfected cells.

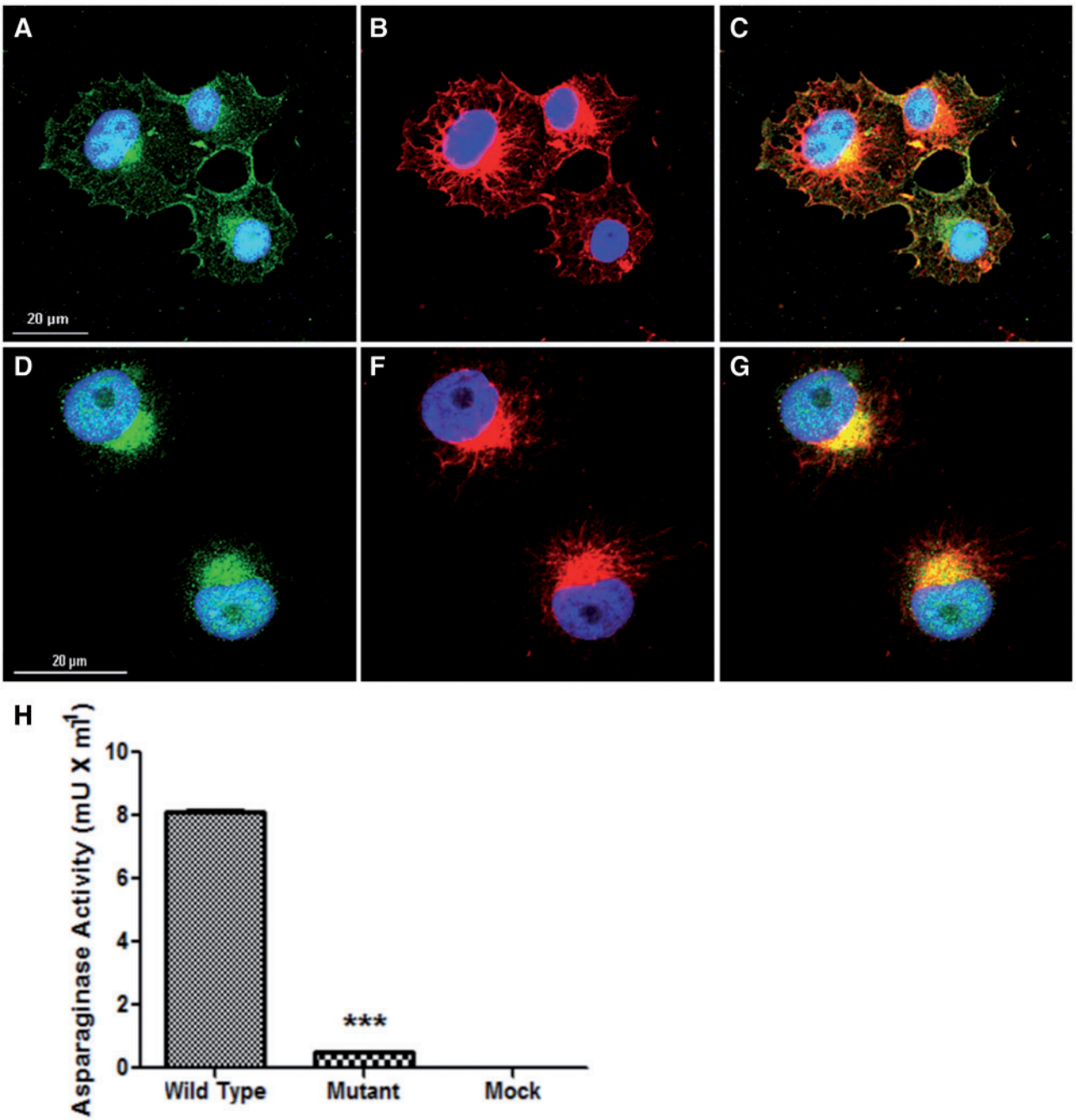

Figure 6. Expression and localization of wt and G178R-ASRGL1 in Cos-7 cells. **(A)** Cos7 cells transfected with wt-*ASRGL1* tagged with cMyc (green), showed the distribution of ASRGL1-cMyc fusion protein throughout the cytoplasm. **(B)** The cytoskeletal marker Vimentin (Red) distributed throughout the cytosol. **(C)** Merged image of A and B. **(D)** The cells transfected with G178R-*ASRGL1* showed perinuclear localization of the G178R-ASRGL1-cMyc fusion protein (green). **(E)** Re-organization of Vimentin signal (Red) in cells transfected with G178R-*ASRGL1*. **(F)** Co-localization of G178R-ASRGL1 and Vimentin. **(G)** Asparaginase activity in the whole cell lysates of cells transfected with wt-*ASRGL1* and G178R-*ASRGL1*. The asparaginase activity detected in cells expressing the G178R-*ASRGL1* was significantly lower ($P < 0.0001$) compared with the enzymatic activity observed in cells expressing the wt-*ASRGL1*.

Zebrafish study

In order to study the effect of *ASRGL1* knockdown on the zebrafish retinal phenotype, we co-injected zebrafish at 1-cell stage with either a start site morpholino (MO) or splice site MO along with a p53 MO to suppress off-target effects caused by MO's (22). Zebrafish co-injected with p53 MO and Asrgl1-start site MO or Asrgl1-splice site MO's at 5 pg concentration had the lowest survival percentage at 6 dpf and resulted in fish with abnormal and deformed phenotypes starting at 1 dpf (Table 4). The axial length of zebrafish injected with 1 pg of start site MO + p53 MO and splice site MO + p53 MO had a higher survival percentage when compared with the fish injected with p53 MO + negative control MO (Table 4).

The Asrgl1-start site MO and splice site MO at 1 pg concentration were able to knockdown the expression of *Asrgl1* transcript, when compared to the negative control MO injected fish

Table 4. Gross morphology and axial length measurements of zebrafish injected with MOs and mRNA

Type of injection	Fish injected (0 dpf)	Fish survived at 6 dpf	Fish survived (%)	Axial length (μM) at 6 dpf	Gross Morphology of fish at 6 dpf
Injection with MO					
Asrgl1-Start site MO 5pg+p53 MO 5pg	60	2	3.33		Abnormal and deformed fish
Asrgl1-Start site MO 3.5pg+ p53 MO 3.5pg	64	21	32.81	234.5 ± 9.85	None
Asrgl1-Start site MO 1pg+3.5pg p53 MO	120	98	81.67	238.80 ± 10.5	None
Asrgl1-Splice site MO 5pg+p53 MO 5pg	65	5	7.69		Abnormal and deformed fish
Asrgl1-Splice site MO 3pg+p53 MO 3.5pg	60	24	40	231.84 ± 7.82	None
Asrgl1-splice site MO 1pg+ p53 MO 3.5pg	60	45	75	234.16 ± 6.86	None
Negative control MO 3.5pg +p53 MO 3.5pg	120	96	80	232.62 ± 7.68	None
Injection with mRNA					
Dye injection	75	53	70.67	232.28 ± 9.4	None
Wt-*ASRGL1* 20 pg	102	75	73.53	233.48 ± 6.5	None
Wt-*ASRGL1* 100 pg	40	36	90	234.24 ± 6.2	None
Wt-*ASRGL1* 200 pg	50	40	80	235.62 ± 7.4	None
G178R-*ASRGL1* 3 pg	101	46	45.54	234.48 ± 8.16	None
G178R-*ASRGL1* 4 pg	100	37	37	220.80 ± 10.13	None
G178R-*ASRGL1* 5 pg	110	32	29.09	185.12 ± 5.38	Fish with small eye phenotype/ abnormality and edema
G178R-*ASRGL1* 6 pg	105	30	28.57	<180	Few zebrafish (n = 5) are significantly deformed and rest had developmental abnormalities
G178R-*ASRGL1* 12 pg	105	8	7.62	<180	Abnormal and deformed fish
G178R-*ASRGL1* 25 pg	45	2	4.44	<180	Abnormal and deformed fish
G178R-*ASRGL1* 50 pg	46	5	10.87	<180	Abnormal and deformed fish
G178R-*ASRGL1* 75 pg	49	4	8.16	<180	Abnormal and deformed fish
G178R-*ASRGL1* 100 pg	50	3	6	<180	Abnormal and deformed fish
G178R-*ASRGL1* 150 pg	54	4	7.41	<180	Abnormal and deformed fish
G178R-*ASRGL1* 200 pg	52	2	3.85	<180	Abnormal and deformed fish

after 24 h of injection (Supplementary Material, Figure S3). The primers designed to amplify nearly 160 bp of the *Asrgl1* transcript near the start site did not detect a band in qRT- polymerase chain reaction (PCR), indicating that the expression of *Asrgl1* was negligible or absent. The splice site Asrgl1 MO reduced the expression of the *Asrgl1* transcript significantly indicating that *Asrgl1* transcript may be unstable and may undergo a nonsense mediated decay, a mechanism that needs further investigation. The knockdown of Asrgl1 transcript in zebrafish did not result in any gross morphological, developmental or axial length (Table 4) when compared with the negative control MO injected fish at 6 dpf.

Evaluation of the retinal morphology of zebrafish injected with 1 pg start site MO, splice site MO and negative control MO at 6 dpf with ND1 antibody (labels rod photoreceptors) and Zpr1 antibody (labels double cone photoreceptors), did not reveal gross morphological abnormalities (data not shown) suggesting that loss of *ASRGL1* may not have a significant effect on the retina of zebrafish at this age.

In order to determine the effect of overexpression of wt and mutant h*ASRGL1* mRNA on the retinal phenotype, zebrafish at the single cell stage (0 dpf) were injected with the above mRNA. The retinal phenotype of these fish was evaluated by studying the retinal morphology and expression of rod and cone specific markers up to 6 dpf.

The zebrafish injected with ≤3 pg of G178R-h*ASRGL1* mRNA did not show alternation in their eye axial length and survival. The fish injected with 4 and 5 pg of G178R-h*ASRGL1* mRNA-exhibited a smaller eye size with decrease axial eye length (220.80 μM ±10.13 for 4 pg injection and 185.12 μM ± 5.38 for 5 pg injection) and elevated mortality with an increase in mRNA concentration at 6 dpf (Table 4). The zebrafish injected with G178R-h*ASRGL1* mRNA at concentrations >6 pg developed severe pathology and mortality in a majority of the fish at 1 dpf, while injection of wt-h*ASRGL1* mRNA at concentrations over 200 pg (40-fold higher) did not affect the retinal morphology or axial length, indicating that wt-h*ASRGL1* mRNA does not exhibit toxicity nor induce abnormal eye phenotype in zebrafish.

The zebrafish injected with 4pg of G178R-h*ASRGL1* mRNA showed smaller eye phenotype (axial length 220 ± 10.13 μM) ($P < 0.005$) with pericardial edema and overall smaller size of the fish when compared with the dye-injected and wt-h*ASRGL1* mRNA (20 pg) injected fish (Supplementary Material, Figure S2C). In G178R-h*ASRGL1* mRNA injected fish, a few to no cells that were positively stained with blue cone opsin antibodies were observed when compared with green and UV opsin expressing cells and rod photoreceptors, indicating the loss of blue cones in these zebrafish. Zebrafish injected with 5pg of G178R-h*ASRGL1* developed severe morphological and developmental abnormalities including smaller eye (axial length < 185μM) ($P < 0.005$) phenotype and edema of the yolk-sack and pericardium. Immunohistochemistry of the retinal sections showed disorganized nuclear layers and rod and cone photoreceptors (Fig. 7). The expression of ASRGL1 in zebrafish could not be analyzed, as antibodies that recognize the zebrafish protein were not available. The G178R-h*ASRGL* mRNA injections at concentrations >6

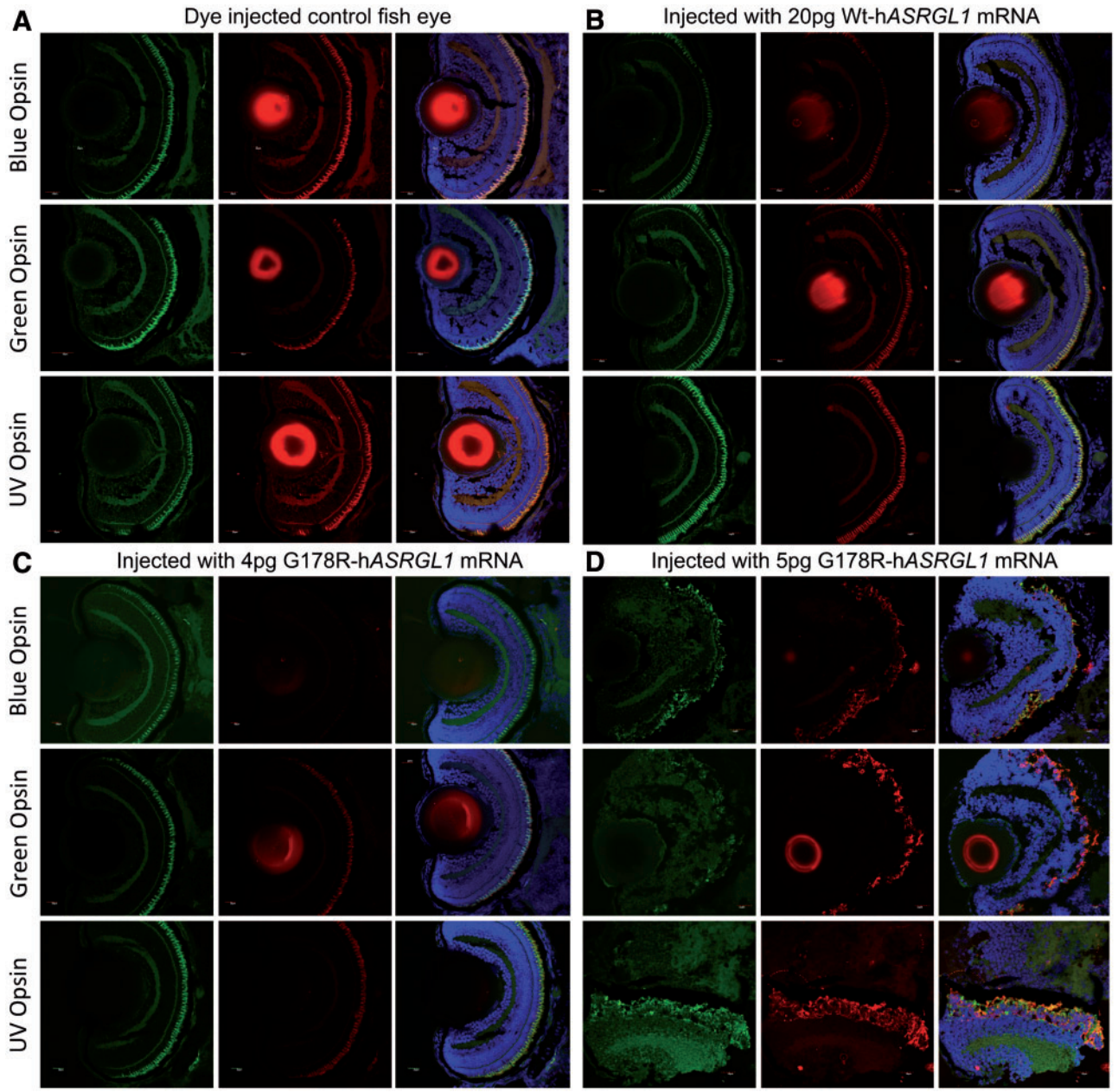

Figure 7. Retinal maker protein expression in zebrafish injected with wt or G178R-*ASRGL1* mRNA. **(A)** Dye-injected fish showing normal distribution of cones. **(B)** Fish injected with 20 pg wt-*ASRGL1* mRNA showed normal pattern of cone distribution. **(C)** Fish injected with only 4 pg G178R-*ASRGL1* mRNA showed loss of green cones. **(D)** Fish injected with 5 pg of G178R-*ASRGL1* mRNA showed eye development abnormality. First column: Immunostaining with rod specific antiobodies (green); Second column: Immunostaining with Blue/Red/UV opsin specific antibodies (Red). The third column in each panel is the merged image of sections stained for rod and cone photoreceptors and the nuclei stained with DAPI.

pg developed severe pathology and mortality at 1 dpf. However, injections with wild-type h*ASRGL1* mRNA at concentrations over 200 pg (40-fold higher) did not develop abnormal phenotype or alteration in the axial length of the fish, indicating that the over expression of G178R-h*ASRGL1* mRNA induces developmental abnormalities and ocular phenotype.

In order to study the effect of *ASRGL1* knockdown on the zebrafish retinal phenotype, we co-injected zebrafish at 0 dpf with either start site MO or splice site MO along with a p53 MO (data not shown). Evaluation of the retinal morphology of these fish at 6 dpf did not reveal gross morphological abnormalities suggesting that loss of functional *ASRGL1* may not have a significant effect on the retina of zebrafish at this age.

Discussion

Linkage and haplotype analysis localized the disease locus in the PKRD104 pedigree to chromosome 11p11.2-q13.1. Exome sequencing and variant analysis identified the c.532G>A; p.G178R mutation in the *ASRGL1* gene segregating with IRD.

The h*ASRGL1* is a member of the N-terminal nucleophile family that catalyzes the hydrolysis of L-asparagine and isoaspartyl-dipeptides (20,21). This enzyme is synthesized as an inactive precursor protein that undergoes autocatalytic intramolecular processing to generate its active form (20). The *ASRGL1* gene has not been implicated in causing pathology including retinal degenerations. The effect of the p.G178R

mutation on h*ASRGL1* and the retinal physiology are not known. We tested the hypothesis that the p.G178R mutation impairs h*ASRGL1* function by expressing the mutant protein in bacteria and mammalian cells. Purification of recombinant G178R-ASRGL1 from *E. coli* showed significant impairment of autocatalytic activation and an accumulation of HMW species, as compared with wt (Fig. 5A). Expression of G178R-ASRGL1 in heterologous cells resulted in altered intracellular localization of the protein and formation of aggresomes (Fig. 6A–F). Furthermore, the zebrafish expressing the G178R-h*ASRGL1* developed retinal abnormalities (Fig. 7) while the knockdown of h*ASRGL1* in zebrafish did not have a significant effect on the retinal phenotype. These data suggest that the p.G178R mutation observed in patients with retinal degeneration is likely to cause misfolding, intracellular misrouting and/or formation of higher molecular weight ASRGL1 aggregates. Protein misfolding and mis-localization have been reported as the primary cause of pathology in band keratopathy, a recessive condition similar to IRD due to the involvement of *ASRGL1* mutation (23). In addition, protein misfolding, intracellular misrouting and accumulation of misfolded proteins in cells have been reported in dominant and recessive retinal degenerations and neurodegenerations (24–26).

The levels of asparaginase activity in the lysates of cells transfected with the mutant *ASRGL1* construct is significantly lower compared with cells expressing the wild-type protein (Fig. 6G). This observation further supports the suggestion that the p.G178R mutation impairs autocatalytic processing, causing the least stable precursor protein to partition to an unfolded/degraded state, with consequent effects on the enzymatic function (Fig. 5C).

The role of asparaginase in retinal tissue is unknown. However, the absence of normal β-aspartyl peptidases may have detrimental consequences in cells. Formation of isoaspartyl peptide bonds is one of the most common sources of non-enzymatic protein damage under physiological conditions, causing decrease/loss of a protein's biological function, alteration of the susceptibility of proteins to proteolytic degradation, and aggregation (27). Accumulation of isoaspartyl peptides in the retina and brain has been reported in aging and neuropathology (28–34). The function of β-aspartyl peptidases, including h*ASRGL1* is the degradation of isoaspartyl peptides (35). Having sub-functional *ASRGL1* due to the p.G178R mutation is likely to result in the improper clearance of isoaspartyl-containing peptides/proteins that may contribute to unfolded protein response or proteasomal overload, which have been implicated in IRD (36–38).

Our studies on the expression and localization of ASRGL1 revealed high levels of expression of this gene in the photoreceptor layer and sustained high levels of its expression in the retina at older ages suggesting a key role for ASRGL1 in maintaining retinal tissue. The impairment in autocatalytic processing of hASRGL1 leading to the formation of high molecular weight protein aggregates or aggresomes due to the homozygous c.532G > A (p.G178R) mutation in the retina may lead to degeneration of photoreceptors, which show high levels of expression of this gene. Alternatively, lack of functional ASRGL1 and accumulation of isoaspartyl peptides might contribute to the retinal degeneration observed in patients with the *ASRGL1* mutation. Expression of ASRGL1 was observed in non-ocular tissue including the brain and heart tissue of mice. However, no non-ocular abnormalities were observed in patients with the homozygous c.532G > A *ASRGL1* mutation suggesting a possible compensation of the loss of functional ASRGL1 in those tissue. The role of h*ASRGL1* in general and its significance in retinal tissue in particular are not known and understanding the molecular mechanism underlying retinal degeneration due to the c.532G > A mutation in this gene will open avenues to gain better insight into the molecular pathology of retinal degenerations.

Methods

Ethics statement

All studies were carried out in accordance with the declaration of Helsinki and with the approval of the institutional review boards of University of California San Diego, La Jolla, CA, Johns Hopkins University, Baltimore, MD and the National Center of Excellence in Molecular Biology, Lahore, Pakistan. Written informed consent was obtained from all participating subjects. Blood samples were collected from thirteen members of a family (PKRD104) from the Punjab province of Pakistan (Fig. 1A).

Clinical studies

Complete ophthalmic examination including measurement of visual acuity, electroretinography (ERG), fundus photography, visual field and color vision test were performed as described earlier (39). Photopic responses were measured at 0 dB while the 30 Hz flicker responses were recorded at 0 dB to a background illumination of 17–34 cd/m^2 using LKC Technologies, Inc. (Gaithersburg, MD).

Genome-wide scan and linkage analysis

Applied Biosystems MD-10 linkage mapping panels (Applied Biosystems, Foster City, CA) were used to complete a genome-wide scan for family PKRD104. Multiplex PCR was completed as described previously in (40). PCR products were mixed with a loading cocktail containing HD-400 size standards (Applied Biosystems) and resolved in an Applied Biosystems 3100 DNA Analyzer. Genotypes were assigned using the Gene Mapper software from Applied Biosystems. Linkage analysis was performed with alleles of PKRD104 obtained through the genome-wide scan using the FASTLINK version of MLINK from the LINKAGE Program Package (41,42). Maximum LOD scores were calculated using ILINK from the LINKAGE Program Package.

Genetic analysis

Exomes of two affected and one unaffected (IV: 2, IV: 7, IV: 8) individuals were captured using the Agilent V5 + UTRs probe capture kit (Fig. 1). Read mapping and variant calling were carried out using BWA and GATK (43). Variants were filtered using exomeSuite as described earlier in (9). Segregation analysis and screening of ethnicity-matched controls was performed by Sanger's di-deoxynucleotide sequencing (44). Mutation analysis of the Bestrophin-1 gene was carried out as described earlier in (45).

Expression of *ASRGL1* transcript

Ocular tissues were dissected from 2-months-old wt C57BL/6 mice. Isolation of RNA, reverse transcription reaction and calculation of *ASRGL1* expression relative to the housekeeping gene *GAPDH* was performed as described earlier in (46).

Immunolocalization in the mouse retina

Immunohistochemistry was performed on cryosections of eyes from 2-months-old wt C57BL/6 mice as described earlier in (47). Rabbit anti-ASRGL1 antibodies (1:100) (ProteinTech Cat-11400-1-AP) and AlexaFluor 488-conjugated donkey anti-rabbit secondary antibody (1:2000) (Invitrogen, Carlsbad, CA, USA) were utilized for staining. Images were captured using Nikon confocal microscope system (A1R+ STORM, Nikon; Melville, NY, USA).

Generation of constructs for bacterial expression

The G178R-*ASRGL1* (mut-*ASRGL1*) and the G178R-(cp)*ASRGL1* constructs were generated by overlap extension PCR using a plasmid containing the human wt *ASRGL1* (wt-*ASRGL1*) and the circularly permuted human wt (cp)*ASRGL1* respectively (wt-p*ASRGL1* and wt-p(*cp*)*ASRGL1* were codon optimized for bacterial expression (20)). The following primers were used for amplification: T7 Forward-5′-TAATACGACTCACTATAGGG-3′, T7 Reverse-5′-TGCTAGTTATTGCTCAGCG-3′ and mut-*ASRGL1* Forward-5′-GGCGCTGTCGCCCTGGACTGCAAGCGCAATGTGGCG TATGCGACC-3′, mut-*ASRGL1* Reverse-5′-GGTCGCATACGC CACATTGGCTTGCAGTCCAGGGCGACAGCGCC-3′. The resulting DNA products were cloned into pET28a (Novagen, Billerica MA, USA) vector. The recombinant plasmids, wt-p*ASRGL1*, wt-p(*cp*)*ASRGL1*, G178R-p*ASRGL1* and G178R-p(cp)*ASRGL1* were sequenced and then transformed into *E. coli* BL21 (DE3) electro-competent cells for protein expression.

Expression in *E. coli* and purification

Transformed *E. coli* BL21 (DE3) cells were cultured overnight and the harvested cells were lysed by passing through a French pressure cell. The cell debris was separated by centrifugation at 24 000 *g* for 20 min and the resulting supernatants containing wt-ASRGL1, G178R-ASRGL1 or G178R-(cp)ASRGL1 proteins were further purified as previously described in (20,21).

In vitro processing of wt-ASRGL1 and G178R-ASRGL1

To evaluate the autocatalytic processing of wt-ASRGL1 and G178R-ASRGL1, aliquots of an equivalent mass of total purified proteins were incubated at 37 °C and at various times, samples were withdrawn and analyzed via SDS-PAGE on a 4-20% precast Tri-Glycine gel (NuSep Ltd.) run under reducing conditions and stained with Coomassie Blue (20). To quantitatively assess intramolecular processing over time, gel band intensities were measured using a densitometry-imaging program.

Kinetic analysis of G178R-(cp)ASRGL1

Reactions of G178R-(cp)ASRGL1 (0.5–1 μM total enzyme) with L-AHA (concentrations from 0 to 5× K_M) were carried out at 25°C in 50 mM HEPES (4-(2-hydroxyethyl)-1-piperazineethanesulfonic acid), 100 mM NaCl, pH 7.4, and the formation of hydroxylamine product was determined by measuring the absorbance at 705 nm as previously reported in (21).

The kinetics of G178R-(cp)ASRGL1 (0.5-1 μM total enzyme) with β-Asp-Phe methyl ester (concentrations from 0 to 5× K_M) were performed at 37°C in 50 mM HEPES, 100 mM NaCl, pH 7.4, and the formation of L-aspartic acid was determined following o-phthalaldehyde-derivatization and HPLC analysis as previously reported in (20). The observed rates were fit to the Michaelis-Menten equation using the program Kaleidagraph (Synergy).

Generation of constructs for mammalian cell transient transfections

The image clone containing full-length human *ASRGL1* (h*ASRGL1*) cDNA (Clone: MGC: 29455; IMAGE: 3937243) was purchased from ATCC (American Type Culture Collection, Manassas, VA). The sequence of the clone was verified using 5′-GTAGTGGTCCAC GGCGGCGGAGCCGGTCCCATCTCCAAGGATCG-3′ forward primer and 5′-GCGTAGGCTACATTCCTTTTGCAGTCCAAGGC-3′ reverse primer. The point mutation (p.G178R) was introduced by site directed mutagenesis using primers 5′-GCCTTGGACTGC AAAAGGAATGTAGCCTACGC-3′ and 5′- GCGTAGGCTACATT CCTTTTGCAGTCCAAGGC-3′. The PCR product was purified using the Zymoclean Gel DNA Recovery Kit (Zymogen Research, Irvine, CA, USA) and ligated using Gibson Assembly Cloning kit (New England BioLabs Inc, MA, USA). Subsequently, the wt-*ASRGL1* and G178R-*ASRGL1* constructs were generated in pDEST40 vector using Multisite gateway Cloning Kit (Life Technologies, Carlsbad, CA, USA). Each construct contained two inserts of h*ASRGL1*. The first copy of h*ASRGL1* was tagged with poly-histidine at the N-terminus and the second copy of h*ASRGL1* was tagged with cMyc tag at the C-terminus.

Subcellular localization and expression of the wt and mutant (G178R) *ASRGL1*

Cos-7 cells and 293-A cells were transfected with recombinant pDEST-expression vectors containing wt/wt or mut/mut inserts using Neon Transfection System (Life Technologies, Carlsbad, CA, USA) as described earlier in (24). After 24 h of transfection, cells were collected for further analysis. Immunofluorescence analysis of transfected cells was carried out as described earlier in (24). Rabbit-anti-cMyc antibody (1:200) (Sigma Aldrich, St Louis, MO, USA), mouse-anti-Vimentin antibodies (1:200) (Sigma Aldrich, St Louis, MO, USA) donkey-anti-mouse Alexa-Fluor-555 (1:3000) (Invitrogen, Carlsbad, CA, USA) and donkey anti-rabbit secondary antibody (1:2000) (Invitrogen, Carlsbad, CA, USA) were used for immunostaining. Images were captured using Nikon confocal microscope system (A1R STORM, Melville, NY, USA). The intracellular localization of wt-ASRGL1 and G178R-ASRGL1 proteins was compared relative to the cytoskeletal marker vimentin.

Quantitation of asparaginase activity

Asparaginase enzymatic activity of the wt and mutant ASRGL1 was measured in the whole cell lysates of 2×10^6 post-transfected cells (transfected with the wt and mutant *ASRGL1* constructs respectively) using Asparaginase Activity Assay Kit (ab107922, Abcam, Cambridge, MA, USA).

Generation and maintenance of Zebrafish cultures

Zebrafish (*Danio rerio*) embryos acquired by natural spawning were maintained at 28.5 °C on a 14-h light/10-h dark cycle in 1× E3 media. Embryos were grown in 10 cm dishes in 1× E3 media supplemented with 0.6 μM methylene blue (Fisher Scientific). The developmental stage was determined by days post fertilization (dpf) as well as by morphological criteria. The laboratory-reared Tuebingen Long-fin strain of zebrafish was used and the studies were carried out on zebrafish embryos from 0 to 6 dpf.

Zebrafish histology and immunohistochemistry

Histological analysis was performed using standard protocols. Briefly, zebrafish (6 dpf) were fixed in 4% paraformaldehyde/PBS and frozen sections were prepared as described earlier in (48). Immunohistochemistry was performed on 8–10 μm cryosections using 4C12 (1:150) (gift from Dr James Fadool), Zpr1 mouse monoclonal antibody (1:150) (ZIRC, OR, USA), anti-green opsin (1:500), anti-blue opsin (1:250), anti-UV opsin (1:1000) (gift from Dr David Hyde), Alexa Fluor 488 chicken anti-mouse IgG (H + L) and Alexa Fluor 594 chicken anti-rabbit IgG (Life Technologies, Carlsbad, CA, USA). Images were captured with an AxioImager Zeiss microscope (Zeiss, Thornwood, NY, USA).

Knockdown of Asrgl1 in zebrafish

MO oligonucleotides were synthesized by Gene Tools (Gene Tools, Philomath, OR). Antisense MO oligonucleotides were designed to target the translation initiation site of zebrafish Asrgl1, 5′- CACCACCACCGGCAGCATATCTGTC -3′, the splice junction between introns 4-5 and exon-5 of *Asrgl1*, 5′-TTCC CCTGGAACACACAAATGAAGA-3′, zebrafish p53, 5′-GCGCCATTG CTTTGCAAGAATTG -3′ to suppress apoptotic effects induced by some MOs and a standard negative control MO, 5′-CCTCTTACCTCAGTTACAATTTATA-3′ (*control-MO*), were used (22). The MOs were solubilized in water and diluted from 0.5 to 3.5 pg with 0.1% phenol red dye for microinjections into embryos. The MOs were heat solubilized by incubating at 65°C for 15 min in order to enable their complete solubulization before diluting them for injections. The MO oligomers (0.5–3.5 pg) were injected alone or by co-injection with p53 MOs into 1 to 2-cell stage embryos as previously described in (22). The efficacy of MO injections was evaluated by semi-quantitative RT-PCR using RNA extracted from injected embryos at 1 dpf and using primer sets to amplify Asrgl1 transcript Asrgl1startsite_MO Fwd, 5′-GAAAGAGGCAGCCAGGACTG-3′ and Asrgl1startsite_MO Rev, 5′-CAATGCATCCATCTCTACCTC-3′; Asrgl1 splice-site_MO Fwd, 5′-GGAAGTGCCCGAGGAGTCATT-3′ and Asrgl1 splice-site_MO Rev 5′- CTTCTCCGTGGCCTGTGGG-3′.

Overexpression of *hASRGL1* in zebrafish

The recombinant wt-h*ASRGL1* and G178R -h*ASRGL1* clones were used to generate the full-length mRNA with the mMESSAGE mMACHINE T7 kit (Invitrogen, Carlsbad, CA, USA) following the manufacturer's instructions. The mRNA was analyzed for size and quality using a Bioanalyzer RNA nano Chip (Agilent, Santa Clara, CA, USA). Each embryo was injected with a specific dose of mRNA (ranging from 1 to 200 pg) of wt-h*ASRGL1* or G178R-h*ASRGL1* mRNA and/or phenol red dye. A dosage curve (1–200 pg) was generated to standardize the concentration of mRNA to be injected into zebrafish embryos to study their eye phenotype.

Measurement of the eye axial length of Zebrafish morphants

Zebrafish (6 dpf) were anesthetized with 0.05% Tricaine-S and the eye size was measured by imaging at a fixed magnification from a dorsal perspective with a Leica DFC425C camera attached to a Leica MZ8 stereo microscope and using Metamorph Basic software (Leica Microsystems Inc., IL, USA). The axial length of each eye from the dorsal view was traced using the Region Measurements function. Nearly 100 pairs of zebrafish eyes were measured for each experiment.

Supplementary Material

Supplementary Material is available at *HMG* online.

Acknowledgements

We would like to thank all the individuals for participating in this research study. We are also grateful to Carlo Rivolta, Department of Medical Genetics, University of Lausanne, Lausanne, Switzerland and Fowzan Alkuray, King Faisal Specialist Hospital and Research Center, Riyadh, Saudi Arabia for screening the database of variants observed in their study cohorts for sequence alterations in *ASRGL1*.

Conflict of Interest statement. None declared.

Funding

This work was supported by; The Foundation Fighting Blindness, Research to Prevent Blindness, Bright Focus Foundation grant, NIH- EY21237, P30-EY22589 CPRIT RP120314.

References

1. Heckenlively, J.R. (1988) *Retinitis Pigmentosa*. J.B. Lippincott Company, Philadelphia.
2. Thompson, D.A., Ali, R.R., Banin, E., Branham, K.E., Flannery, J.G., Gamm, D.M., Hauswirth, W.W., Heckenlively, J.R., Iannaccone, A., Jayasundera, K.T., *et al*. (2015) Advancing therapeutic strategies for inherited retinal degeneration: recommendations from the Monaciano Symposium. *Investigative Ophthalmology and Visual Science*, **56**, 918–931.
3. Wert, K.J., Lin, J.H. and Tsang, S.H. (2014) General pathophysiology in retinal degeneration. *Dev. Ophthalmol.*, **53**, 33–43.
4. Roosing, S., Thiadens, A.A., Hoyng, C.B., Klaver, C.C., den Hollander, A.I. and Cremers, F.P. (2014) Causes and consequences of inherited cone disorders. *Prog. Retin. Eye Res.*, **42**, 1–26.
5. Sahel, J.A., Marazova, K. and Audo, I. (2015) Clinical characteristics and current therapies for inherited retinal degenerations. *Cold Spring Harb. Perspect. Med.*, **5**, a017111.
6. Farber, D.B., Heckenlively, J.R., Sparkes, R.S. and Bateman, J.B. (1991) Molecular genetics of retinitis pigmentosa. *West. J. Med.*, **155**, 388–399.
7. Maria, M., Ajmal, M., Azam, M., Waheed, N.K., Siddiqui, S.N., Mustafa, B., Ayub, H., Ali, L., Ahmad, S., Micheal, S., *et al*. (2015) Homozygosity mapping and targeted sanger sequencing reveal genetic defects underlying inherited retinal disease in families from pakistan. *PloS One*, **10**, e0119806.
8. Maranhao, B., Biswas, P., Duncan, J.L., Branham, K.E., Silva, G.A., Naeem, M.A., Khan, S.N., Riazuddin, S., Hejtmancik, J.F., Heckenlively, J.R., *et al*. (2014) exomeSuite: Whole exome sequence variant filtering tool for rapid identification of putative disease causing SNVs/indels. *Genomics*, **103**, 169–176.
9. McKibbin, M., Ali, M., Mohamed, M.D., Booth, A.P., Bishop, F., Pal, B., Springell, K., Raashid, Y., Jafri, H. and Inglehearn, C.F. (2010) Genotype-phenotype correlation for leber congenital amaurosis in Northern Pakistan. *Arch. Ophthalmol.*, **128**, 107–113.
10. Li, D., Jin, C., Jiao, X., Li, L., Bushra, T., Naeem, M.A., Butt, N.H., Husnain, T., Sieving, P.A., Riazuddin, S., *et al*. (2014) AIPL1 implicated in the pathogenesis of two cases of autosomal recessive retinal degeneration. *Mol. Vis.*, **20**, 1–14.
11. Naeem, M.A., Chavali, V.R., Ali, S., Iqbal, M., Riazuddin, S., Khan, S.N., Husnain, T., Sieving, P.A., Ayyagari, R.,

Riazuddin, S., *et al.* (2012) GNAT1 associated with autosomal recessive congenital stationary night blindness. *Invest. Ophthalmol. Vis. Sci.*, **53**, 1353–1361.
12. Riazuddin, S.A., Iqbal, M., Wang, Y., Masuda, T., Chen, Y., Bowne, S., Sullivan, L.S., Waseem, N.H., Bhattacharya, S., Daiger, S.P., *et al.* (2010) A splice-site mutation in a retina-specific exon of BBS8 causes nonsyndromic retinitis pigmentosa. *Am. J. Hum. Genet.*, **86**, 805–812.
13. Riazuddin, S.A., Shahzadi, A., Zeitz, C., Ahmed, Z.M., Ayyagari, R., Chavali, V.R., Ponferrada, V.G., Audo, I., Michiels, C., Lancelot, M.E., *et al.* (2010) A mutation in SLC24A1 implicated in autosomal-recessive congenital stationary night blindness. *Am. J. Hum. Genet.*, **87**, 523–531.
14. El-Asrag, M.E., Sergouniotis, P.I., McKibbin, M., Plagnol, V., Sheridan, E., Waseem, N., Abdelhamed, Z., McKeefry, D., Van Schil, K., Poulter, J.A., *et al.* (2015) Biallelic mutations in the autophagy regulator DRAM2 cause retinal dystrophy with early macular involvement. *Am. J. Hum. Genet.*, **96**, 948–954.
15. Maranhao, B., Biswas, P., Gottsch, A.D., Navani, M., Naeem, M.A., Suk, J., Chu, J., Khan, S.N., Poleman, R., Akram, J., *et al.* (2015) Investigating the molecular basis of retinal degeneration in a familial cohort of Pakistani decent by exome sequencing. *PloS One*, **10**, e0136561.
16. MacDonald, I.M., Gudiseva, H.V., Villanueva, A., Greve, M., Caruso, R. and Ayyagari, R. (2012) Phenotype and genotype of patients with autosomal recessive bestrophinopathy. *Ophthalmic Genet.*, **33**, 123–129.
17. Burgess, R., Millar, I.D., Leroy, B.P., Urquhart, J.E., Fearon, I.M., De Baere, E., Brown, P.D., Robson, A.G., Wright, G.A., Kestelyn, P., *et al.* (2008) Biallelic mutation of BEST1 causes a distinct retinopathy in humans. *Am. J. Hum. Genet.*, **82**, 19–31.
18. Petrukhin, K., Koisti, M.J., Bakall, B., Li, W., Xie, G., Marknell, T., Sandgren, O., Forsman, K., Holmgren, G., Andreasson, S., *et al.* (1998) Identification of the gene responsible for Best macular dystrophy. *Nat. Genet.*, **19**, 241–247.
19. Marquardt, A., Stohr, H., Passmore, L.A., Kramer, F., Rivera, A. and Weber, B.H. (1998) Mutations in a novel gene, VMD2, encoding a protein of unknown properties cause juvenile-onset vitelliform macular dystrophy (Best's disease). *Hum. Mol. Genet.*, **7**, 1517–1525.
20. Cantor, J.R., Stone, E.M., Chantranupong, L. and Georgiou, G. (2009) The human asparaginase-like protein 1 hASRGL1 is an Ntn hydrolase with beta-aspartyl peptidase activity. *Biochemistry*, **48**, 11026–11031.
21. Li, W., Cantor, J.R., Yogesha, S., Yang, S., Chantranupong, L., Liu, J.Q., Agnello, G., Georgiou, G., Stone, E.M. and Zhang, Y. (2012) Uncoupling intramolecular processing and substrate hydrolysis in the N-terminal nucleophile hydrolase hASRGL1 by circular permutation. *ACS Chem. Biol.*, **7**, 1840–1847.
22. Robu, M.E., Larson, J.D., Nasevicius, A., Beiraghi, S., Brenner, C., Farber, S.A. and Ekker, S.C. (2007) p53 activation by knockdown technologies. *PLoS Genet.*, **3**, e78.
23. Zhang, N., Tsybovsky, Y., Kolesnikov, A.V., Rozanowska, M., Swider, M., Schwartz, S.B., Stone, E.M., Palczewska, G., Maeda, A., Kefalov, V.J., *et al.* (2015) Protein misfolding and the pathogenesis of ABCA4-associated retinal degenerations. *Hum. Mol. Genet.*, **24**, 3220–3237.
24. Vasireddy, V., Vijayasarathy, C., Huang, J., Wang, X.F., Jablonski, M.M., Petty, H.R., Sieving, P.A. and Ayyagari, R. (2005) Stargardt-like macular dystrophy protein ELOVL4 exerts a dominant negative effect by recruiting wild-type protein into aggresomes. *Mol. Vis.*, **11**, 665–676.
25. Schapira, A.H., Olanow, C.W., Greenamyre, J.T. and Bezard, E. (2014) Slowing of neurodegeneration in Parkinson's disease and Huntington's disease: future therapeutic perspectives. *Lancet*, **384**, 545–555.
26. Li, S., Hu, J., Jin, R.J., Aiyar, A., Jacobson, S.G., Bok, D. and Jin, M. (2015) Temperature-sensitive retinoid isomerase activity of RPE65 mutants associated with Leber Congenital Amaurosis. *J. Biochem.*, **158**, 115–125.
27. Aswad, D.W., Paranandi, M.V. and Schurter, B.T. (2000) Isoaspartate in peptides and proteins: formation, significance, and analysis. *J. Pharm. Biomed. Anal.*, **21**, 1129–1136.
28. Qin, Z., Yang, J., Klassen, H. and Aswad, D.W. (2014) Isoaspartyl Protein Damage and Repair in Mouse Retina. *Invest. Ophthalmol. Vis. Sci.*, **55**, 1572–1579.
29. Reissner, K.J., Paranandi, M.V., Luc, T.M., Doyle, H.A., Mamula, M.J., Lowenson, J.D. and Aswad, D.W. (2006) Synapsin I is a major endogenous substrate for protein L-isoaspartyl methyltransferase in mammalian brain. *J. Biol. Chem.*, **281**, 8389–8398.
30. Zhu, J.X., Doyle, H.A., Mamula, M.J. and Aswad, D.W. (2006) Protein repair in the brain, proteomic analysis of endogenous substrates for protein L-isoaspartyl methyltransferase in mouse brain. *J. Biol. Chem.*, **281**, 33802–33813.
31. McFadden, P.N. and Clarke, S. (1982) Methylation at D-aspartyl residues in erythrocytes: possible step in the repair of aged membrane proteins. *Proc. Natl. Acad. Sci. U S A*, **79**, 2460–2464.
32. Vigneswara, V., Cass, S., Wayne, D., Bolt, E.L., Ray, D.E. and Carter, W.G. (2013) Molecular ageing of alpha- and Beta-synucleins: protein damage and repair mechanisms. *PLoS One*, **8**, e61442.
33. Vigneswara, V., Lowenson, J.D., Powell, C.D., Thakur, M., Bailey, K., Clarke, S., Ray, D.E. and Carter, W.G. (2006) Proteomic identification of novel substrates of a protein isoaspartyl methyltransferase repair enzyme. *J. Biol. Chem.*, **281**, 32619–32629.
34. Qin, Z., Dimitrijevic, A. and Aswad, D.W. (2015) Accelerated protein damage in brains of PIMT+/- mice; a possible model for the variability of cognitive decline in human aging. *Neurobiol. Aging*, **36**, 1029–1036.
35. Böhme, L., Bär, J.W., Hoffmann, T., Manhart, S., Ludwig, H.H., Rosche, F. and Demuth, H.U. (2008) Isoaspartate residues dramatically influence substrate recognition and turnover by proteases. *Biol. Chem.*, **389**, 1043–1053.
36. Zhang, S.X., Sanders, E., Fliesler, S.J. and Wang, J.J. (2014) Endoplasmic reticulum stress and the unfolded protein responses in retinal degeneration. *Exp. Eye Res.*, **125**, 30–40.
37. Tzekov, R., Stein, L. and Kaushal, S. (2011) Protein misfolding and retinal degeneration. *Cold Spring Harb. Perspect. Biol.*, **3**, a007492.
38. Lobanova, E.S., Finkelstein, S., Skiba, N.P. and Arshavsky, V.Y. (2013) Proteasome overload is a common stress factor in multiple forms of inherited retinal degeneration. *Proc. Natl. Acad Sci. U S A*, **110**, 9986–9991.
39. Li, L., Nakaya, N., Chavali, V.R., Ma, Z., Jiao, X., Sieving, P.A., Riazuddin, S., Tomarev, S.I., Ayyagari, R., Riazuddin, S.A., *et al.* (2010) A mutation in ZNF513, a putative regulator of photoreceptor development, causes autosomal-recessive retinitis pigmentosa. *Am. J. Hum. Genet.*, **87**, 400–409.
40. Naeem, M.A., Gottsch, A.D., Ullah, I., Khan, S.N., Husnain, T., Butt, N.H., Qazi, Z.A., Akram, J., Riazuddin, S., Ayyagari, R., *et al.* (2015) Mutations in GRM6 identified in consanguineous Pakistani families with congenital stationary night blindness. *Mol. Vis.*, **21**, 1261–1271.
41. Lathrop, G.M. and Lalouel, J.M. (1984) Easy calculations of lod scores and genetic risks on small computers. *Am. J. Hum. Genet.*, **36**, 460–465.

42. Schaffer, A.A., Gupta, S.K., Shriram, K. and Cottingham, R.W. Jr. (1994) Avoiding recomputation in linkage analysis. *Hum. Hered.*, **44**, 225–237.
43. Duncan, J.L., Roorda, A., Navani, M., Vishweswaraiah, S., Syed, R., Soudry, S., Ratnam, K., Gudiseva, H.V., Lee, P., Gaasterland, T., *et al.* (2012) Identification of a novel mutation in the CDHR1 gene in a family with recessive retinal degeneration. *Arch. Ophthalmol.*, **130**, 1301–1308.
44. Duncan, J.L., Navani, M., Vishveswaraiah, S., Gudiseva, H.V., Lee, P., Gaasterland, T. and Ayyagari, R. (2012) Exome analysis identified a novel mutation in a family with recessive retinal degeneration. *ARVO Meet. Abst.*, **53**, 4523.
45. Caldwell, G.M., Kakuk, L.E., Griesinger, I.B., Simpson, S.A., Nowak, N.J., Small, K.W., Maumenee, I.H., Rosenfeld, P.J., Sieving, P.A., Shows, T.B., *et al.* (1999) Bestrophin gene mutations in patients with Best vitelliform macular dystrophy. *Genomics*, **58**, 98–101.
46. Mandal, M.N., Vasireddy, V., Jablonski, M.M., Wang, X., Heckenlively, J.R., Hughes, B.A., Reddy, G.B. and Ayyagari, R. (2006) Spatial and temporal expression of MFRP and its interaction with CTRP5. *Invest. Ophthalmol. Vis. Sci.*, **47**, 5514–5521.
47. Chavali, V.R., Khan, N.W., Cukras, C.A., Bartsch, D.U., Jablonski, M.M. and Ayyagari, R. (2011) A CTRP5 gene S163R mutation knock-in mouse model for late-onset retinal degeneration. *Hum. Mol. Genet.*, **20**, 2000–2014.
48. Uribe, R.A. and Gross, J.M. (2007) Immunohistochemistry on cryosections from embryonic and adult zebrafish eyes. *CSH Protoc.*, **2007**, pdb prot4779.